

# Simulating the magnetized liner inertial fusion plasma confinement with smaller-scale experiments

D. D. Ryutov,<sup>1</sup> M. E. Cuneo,<sup>2</sup> M. C. Herrmann,<sup>2</sup> D. B. Sinars,<sup>2</sup> and S. A. Slutz<sup>2</sup>

<sup>1</sup>Lawrence Livermore National Laboratory, Livermore, California 94551, USA

<sup>2</sup>Sandia National Laboratories, Albuquerque, New Mexico 87185, USA

(Received 13 March 2012; accepted 15 May 2012; published online 20 June 2012)

The recently proposed magnetized liner inertial fusion approach to a Z-pinch driven fusion [Slutz *et al.*, Phys. Plasmas **17**, 056303 (2010)] is based on the use of an axial magnetic field to provide plasma thermal insulation from the walls of the imploding liner. The characteristic plasma transport regimes in the proposed approach cover parameter domains that have not been studied yet in either magnetic confinement or inertial confinement experiments. In this article, an analysis is presented of the scalability of the key physical processes that determine the plasma confinement. The dimensionless scaling parameters are identified and conclusion is drawn that the plasma behavior in scaled-down experiments can correctly represent the full-scale plasma, provided these parameters are approximately the same in two systems. This observation is important in that smaller-scale experiments typically have better diagnostic access and more experiments per year are possible. © 2012 American Institute of Physics. [<http://dx.doi.org/10.1063/1.4729726>]

## I. INTRODUCTION

The recently proposed MagLIF (magnetized liner inertial fusion) concept is based on compressing magnetized fusion fuel plasma using a current-driven cylindrical liner implosion.<sup>1</sup> The magnetized fuel density in MagLIF will be much higher than in typical experiments on magnetic confinement fusion<sup>2</sup> and it will be much lower than in laser-driven inertial confinement fusion experiments.<sup>3</sup> Accordingly, characteristic time-scales will lie in between the time-scales typical for magnetic confinement fusion, which are, roughly, 1–10 s, and those typical for inertial confinement fusion, which are  $\sim 10^{-9}$  s. The plasma in the MagLIF approach will be imploded at a velocity much smaller than the plasma sound velocity and will, therefore, pass through a sequence of radial equilibria supported by the heavy liner. In order to maintain the heat loss to the liner surface at an acceptable level, an axial magnetic field will be used to suppress the heat conduction to the liner-plasma interface. The heat loss to the ends remains uninhibited, but it can be made tolerable by using sufficiently long liners. For realistic lengths, the implosion time would have to be in the range of  $\sim 100$  ns, which is achievable with the drivers of the scale of a Z facility at Sandia.<sup>4</sup> In this regard, the MagLIF concept is different from several other approaches to the liner-compressed plasma, which use slower liners and, therefore, have to rely on a 3-dimensional plasma thermal insulation from the cold liner (e.g., Refs. 5–8 and references therein). The physics of the closed magnetic field line configurations (in particular, field-reversed configuration (FRC)) has a number of features that would require separate analysis going beyond the scope of this paper (see also Sec. IV).

The plasma behavior in the imploding liner is one of the factors defining the success or failure of the MagLIF approach. Systematic studies of the plasma confinement on a full-scale MagLIF experiment on the Z facility will be hindered by the difficulties of the diagnostic access and

relatively low shot rate. It is, therefore, important to identify the conditions in which certain aspects of an overall confinement problem could be studied at smaller-scale facilities. While there is no way to produce exactly the same plasma on a smaller-scale facility, by identifying the proper scaling parameters it may be possible to find conditions where a smaller-scale experiment would be able to properly assess some of the controlling phenomena. This scaling study is the main goal of our paper. For other examples of scalings for time-evolving high-energy-density plasmas, see Refs. 9 and 10 and references therein.

In the course of one implosion, the plasma passes through a sequence of different confinement regimes. Reproducing a complete sequence of these regimes in one scaled-down experiment is hardly possible, as they are very different in the sense of governing parameters, and we suggest a different approach, where scaled-down experiments would imitate the plasma confinement during limited segments of the implosion process. Then, the set of such experiments would cover the whole implosion process.

In the current-driven liner implosions, the plasma pressure is typically less than the external magnetic field pressure until the time immediately preceding the stagnation point: at this last segment, the plasma pressure rapidly reaches the values exceeding the external pressure and the liner slows down and rebounds. A very convenient analytical expression for the 1D liner trajectory has been suggested in Ref. 11 for a power-law time dependence of the implosion current. This expression is quite useful for the general assessment of the desirable parameters of the liner and the current drive.

The overall success of the MagLIF concept depends not only on the plasma performance but also on the quality of the liner implosion, in particular the liner stability. This part of the problem is governed by an entirely different set of parameters, such as the liner equation of state, liner conductivity, liner material strength and others and cannot be folded into the plasma physics analysis. We do not consider liner

stability here, assuming that the liner behaves well-enough. Early encouraging experimental results on the liner stability are presented in Refs. 12 and 13.

If the liner performs as anticipated, it moves much more slowly than the plasma sound speed of the fuel. In particular, at the time when the preliminary plasma with the temperature of 300 eV is created, the liner velocity is below  $4 \times 10^6$  cm/s, whereas the sound speed in a DT plasma is  $2 \times 10^7$  cm/s. Likewise, the liner velocity a few nanoseconds before the rebound is below  $10^7$  cm/s, whereas the sound speed in the 8 keV plasma is  $10^8$  cm/s. This allows us to conceptually frame the problem as the study of plasma transport in the presence of a quasi-stationary wall. For the relatively fast plasma instabilities, we are concerned with here, the motion of the wall is fairly irrelevant.

The rest of the paper is organized as follows. In Sec. II, we identify four dimensionless parameters whose constancy between two plasmas guarantees the similarity of the physical processes, up to the scale transformations of spatial coordinates and time. In Sec. III, some derived dimensionless parameters characterizing specific plasma processes are evaluated. In Sec. IV, our scaling approach is used to assess the feasibility of smaller-scale experiments that would be a scaled-down analogue of the real plasma. We emphasize that our paper does not contain an answer to the question of the plasma confinement times. It just identifies the necessary parameters for smaller-scale experiments to be able to provide answers in lieu of a full scale test. In Sec. V, we analyze the possible further energy saving by switching from deuterium to hydrogen. Finally, Sec. VI contains discussion of our results. A more formal proof of the scalability is presented in Appendix.

## II. DIMENSIONLESS SCALING PARAMETERS

The plasma parameters in a MagLIF implosion vary significantly during the course of the implosion. Their values for a typical implosion are presented in Table I based on Ref. 1. The first line in Table I corresponds to the early time, pre-heated plasma, just created inside the liner by some auxiliary power source (such as an energetic pulsed laser as proposed in Ref. 1). The second line corresponds to the point of the maximum compression of the fusion fuel by the liner. These are representative parameters and are not necessarily those optimized for the best performance; they just provide guidance for the scaling analysis. The parameter  $\tau^*$  in the middle column represents a rough estimate of the time the system spends near the chosen point based on the simulations of Ref. 1. The plasma confinement time must be longer than

this time for the system to work. The meaning of the parameters on the right side of the table will be discussed shortly.

As we will show, the plasma in MagLIF is highly collisional in that the time  $\tau^*$  is much longer than the electron-ion energy exchange time  $\tau_{ei}^{(E)}$ . For this reason, we characterize the plasma by a single temperature  $T$ . The other plasma parameters are the plasma density  $n$  and the magnetic field strength  $B$ ; the geometrical parameters are the plasma radius  $a$  and the plasma length  $L$ . So, the full set of parameters defining the initial plasma state is

$$n, T, B, L, a. \quad (1)$$

By “dialing in” these five parameters, one defines the further evolution of the plasma, including the possible formation of a denser colder plasma in the transition zone to the colder liner. But our main concern will be the region of the hotter plasma where the appearance of an anomalous cross-field transport and strong distortion of the confining magnetic field is a distinct possibility (e.g., Refs. 14–16). A good confinement of the hot plasma, in the region where the temperature decreases by a factor of 5 to 10 from its maximum value on axis is a necessary condition for the MagLIF concept to work.

In a scaled experiment, by creating plasma in some initial state and then allowing it to evolve, one would obtain the information on the characteristic decay time, as well as more subtle features, such as the most prevalent instability modes (if any). The outcome of this experiment is entirely determined by the initial values of  $n$ ,  $T$ ,  $B$ , plus geometrical parameters  $a$ , and  $L$ . If the scaling parameters that we identify below are held the same between the two plasmas, their behavior will be identical, just temporal and spatial scales change.

The fusion fuel plasma is supposed to be an equi-molar mixture of deuterium and tritium; we characterize it by the ion mass  $m_i$  equal to 2.5 proton mass  $m_p$ . For evaluating the ion thermal speed  $V_{Ti} = \sqrt{2T/m_i}$  and the ion gyro-radius  $\rho_i = V_{Ti}/\omega_{Ci}$  (with  $\omega_{Ci}$  being the ion cyclotron frequency), we use the following numerical expressions:

$$\begin{aligned} v_{Ti}(\text{cm/s}) &\approx 2.78 \cdot 10^7 \sqrt{T(\text{keV})}; \\ \rho_i(\mu\text{m}) &\approx 72.1 \sqrt{T(\text{keV})}/B(\text{MG}). \end{aligned} \quad (2)$$

The electron gyro-radius  $\rho_e$  is equal to  $\sqrt{\mu\rho_i}$ , with  $\mu = m_e/m_i = 1/4610$ . When evaluating the Coulomb mean-free-path  $\lambda$ , we ignore the dependence of the Coulomb logarithm on plasma parameters and use the following expression:

$$\lambda(\mu\text{m}) \approx 3 \cdot 10^{22} [T(\text{keV})]^2 / n(\text{cm}^{-3}). \quad (3)$$

For the general scaling analysis, where the parameters vary by several orders of magnitude, the use of these rough expressions is sufficient. Equations (2) and (3) have been used for filling out the corresponding columns in Table I. The plasma energy content that enters the Table is defined as  $W = \pi a^2 L \times 3nT$  (i.e., it accounts for the contributions of both electrons and ions) and is numerically evaluated as

TABLE I. Characteristic plasma parameters for two stages of the implosion: right after creating the pre-heated plasma (1) and at the maximum compression (2). The last 4 columns represent parameters evaluated by Eqs. (2)–(4) and (6).

	$n$ , $10^{21} \text{ cm}^{-3}$	$T$ (keV)	$B$ (MG)	$a$ (mm)	$L$ (mm)	$\tau^*$ (ns)	$\tau$ (ns)	$\rho_i$ ( $\mu\text{m}$ )	$\lambda$ ( $\mu\text{m}$ )	$W$ (kJ)
1	0.3	0.3	0.3	3	6	20	19.7	132	9	7.34
2	120	8	130	0.12	6	2	0.153	1.57	16	125

$$W(\text{kJ}) = 1.51 \cdot 10^{-21} n(\text{cm}^{-3}) T(\text{keV}) [a(\text{mm})]^2 L(\text{mm}), \quad (4)$$

with the temperature, density, and geometrical parameters as in other columns of the Table. The electron-ion energy exchange time is defined as

$$\tau_{ei}^{(E)} = (\lambda / \sqrt{\mu} v_{Ti}) \quad (5)$$

It is indeed quite short compared to the anticipated confinement times, thereby justifying the use of a model that assumes equal electron and ion temperatures.

To find the conditions under which two initial plasmas with different set of initial parameters and different  $a$  and  $L$  evolve similarly (i.e., their spatio-temporal evolution is the same up to some scaling factors), it is convenient to measure the distances in terms of a parameter  $a$  and the time in terms of the acoustic time

$$\tau = a / v_{Ti}. \quad (6)$$

We introduce the following dimensionless scaling parameters:

$$R_1 = \frac{a}{\rho_i}; \quad R_2 = \frac{a}{\lambda}; \quad R_3 \equiv \beta = \frac{16\pi n T}{B^2}; \quad R_4 = L/a. \quad (7)$$

The numerical values of tau are illustrated in Table I. Since the number of input parameters (1) is 5, specifying the radius and 4 dimensionless parameters (7) is equivalent to specifying the 5 input parameters (1). Specifically,

$$n(\text{cm}^{-3}) = 6.43 \cdot 10^{16} \frac{\beta R_1^2}{[a(\text{mm})]^2};$$

$$T(\text{keV}) = \frac{0.0463}{\sqrt{a(\text{mm})}} R_1 \sqrt{\frac{\beta}{R_2}}; \quad (8)$$

$$B(\text{MG}) = \frac{1.55 \cdot 10^{-2} R_1^{3/2} \beta^{1/4}}{[a(\text{mm})]^{5/4} R_2^{1/4}}; \quad L = R_4 a. \quad (9)$$

The Jacobian of the transformation (7) from five input variables (1) to the four dimensionless parameters defined in Eq. (7) and  $a$  is expressly non-zero,  $\partial(n, T, B, L, a) / \partial(R_1, R_2, R_3, R_4, a) = n T B L / 2 R_1 R_2 R_3 R_4$ , meaning that the dimensionless parameters are independent.

The unit of the time (6) is also uniquely defined in terms of the parameters (7) and radius  $a$ :

$$\tau(\text{ns}) = 16.7 [a(\text{mm})]^{5/4} \frac{R_2^{1/4}}{\beta^{1/4} R_1^{1/2}}. \quad (10)$$

We emphasize that  $\tau$  is just a convenient unit of time, not the plasma confinement time, which has to be much longer to be of interest for MagLIF and which, as we show, can be determined from the scaled experiments.

The set of Eqs. (7)–(9) allows one to identify all the systems that would evolve similarly to the initial one: to do that, one has to take the main dimensionless parameters the same, and vary  $a$ . [Instead of parameters defined in Eq. (7), one could choose their other independent combinations such as a

quadruplet of parameters  $R_1 R_2$ ,  $R_1 / R_2$ ,  $R_3$ , and  $R_4$ . We have chosen our parameter definitions (7) because each has a simple physical meaning.] The plasma energy (4) can be represented as

$$W(\text{kJ}) = 4.6 \cdot 10^{-6} \frac{\beta^{3/2} R_1^3 R_4}{\sqrt{R_2}} \sqrt{a(\text{mm})}. \quad (11)$$

In Table II, we present numerical values of scaling parameters corresponding to rows 1 and 2 of Table I. It goes without saying that, if one substitutes for  $a$  the value from Table I and for the dimensionless parameters their values from Table II, one obtains for  $W$ ,  $n$ ,  $T$ ,  $B$ , and  $\tau$  their values from Table I (up to the rounding errors).

One can see that in the first stage, the ions are unmagnetized in the sense that their mean-free path is much shorter than their gyro-radius,  $R_2 \gg R_1$ . The electrons, whose gyro-radii are 70 times smaller, are still magnetized. In combination with a very high plasma beta, this creates an interesting regime that has not yet been studied in any detail either theoretically or experimentally.

During the second stage, the ions are strongly magnetized and their radial thermal conduction is strongly suppressed. On the other hand, as we will show shortly, the collision frequency still remains high compared to the drift frequency, thereby bringing this regime close to that considered theoretically in Refs. 15 and 16. We are not aware of any experimental studies of the  $\beta \gg 1$  plasma transport in this regime. The parallel confinement is collisional in both cases: the mean-free path is much shorter than  $L$ .

Assuming no significant turbulence allows one to describe the confinement classically using the axisymmetric, two dimensional ( $r$ - $z$ ) Braginski equations.<sup>21</sup> These assumptions lead to favorable predictions with regard to the plasma states achievable in MagLIF implosions.<sup>1</sup> On the other end of the spectrum of confinement scenarios is that of anomalous plasma transport driven by substantially 3-dimensional turbulence. As a reference point for the resulting anomalous transport coefficients, the Bohm diffusion coefficient is often used, defined as (in CGS)

$$D_B = \frac{1}{16} \frac{c T}{e B}. \quad (12)$$

One should emphasize that the anomalous transport produced by drift turbulence in collisionless plasma can give rise to transport coefficients exceeding Eq. (12) by an order of magnitude and, possibly, more,<sup>14</sup> making it hard to obtain the temperatures of 5-8 keV needed for reaching the fusion breakeven. In the collisional case considered in Refs. 15 and 16, the predictions are much more favorable.

TABLE II. Scaling parameters (6) for the two stages of the pinch implosion.

	$R_1 = \frac{a}{\rho_i}$	$R_2 = \frac{a}{\lambda}$	$R_3 = \beta$	$R_4 = \frac{L}{a}$
1	22.7	333	80.5	2
2	76.4	7.50	4.57	50

Mesoscale plasma turbulence in a high-beta plasma may lead also to tangling of the imposed axial magnetic field. There are many potential sources for this effect, in particular, a parallel heat flux in a high-beta plasma, coupled with the magnetic field effects on the electron heat conduction and thermal force.<sup>17,18</sup> One more source of the magnetic field perturbations is drift turbulence in a high-beta plasma.<sup>15,16</sup> In both cases, the fastest-growing modes have the spatial scale exceeding the Coulomb mean-free path but small compared to the global scale. The tangled field may, on the one hand, reduce the axial electron heat flux<sup>19</sup> and, on the other hand, increase the radial heat flux.<sup>20</sup> We emphasize that our approach does not allow us to predict the magnitude of these effects in any particular system. What we demonstrate is that all the features of these phenomena (e.g., spectra of magnetic fluctuations) are the same, up to scaling transformations, in two systems, provided the scaling parameters are the same or almost the same.

This discussion shows the richness of the physics effects that may show up in the virtually unexplored domain of plasma parameters. The focus of our paper is on finding out whether one can experimentally study the transport coefficients in the smaller, less energy-intensive experiments than a full-scale MagLIF, and still be confident that an extrapolation to MagLIF is reliable. So, we resort to the scaling analysis to find out the requirements under which these smaller experiments would correctly replicate the full-scale one.

### III. DERIVED DIMENSIONLESS PARAMETERS

Since the set of parameters defined in Eq. (7) and the radius  $a$  fully determine the required initial plasma state, all other characteristic dimensionless parameters can be expressed in terms of this set. As an example, we evaluate the product of the characteristic frequency of the large-scale drift vortices  $\omega_D$  and the electron-ion energy equilibration time  $\tau_{ei}^{(E)}$ . We estimate the first one as

$$\omega_D = \frac{\rho_i}{a} \frac{V_{Ti}}{a} \quad (13)$$

(see, e.g., Ref. 15 and references therein). The second one can be estimated via Eq. (5). The product is the dimensionless parameter

$$\omega_D \tau_{ei}^{(E)} \equiv S_1 = \frac{1}{\sqrt{\mu} R_1 R_2} \quad (14)$$

Note that the drift frequency can be expressed in terms of the Bohm diffusion coefficient (12): using equations  $V_{Ti} = \sqrt{2T/m_i}$  and  $\rho_i = V_{Ti}/\omega_{Ci}$ , one finds that  $\omega_D^{-1} = a^2/(32 D_B)$ . In other words,  $\omega_D^{-1}$  corresponds to a diffusion time over the radius  $a$  for diffusion coefficient, which is more than 10 times higher than the Bohm diffusion coefficient (12). Still, the dimensionless parameter  $S_1$  is small (Table III), meaning that the electron and ion temperature would remain equal to each other even for a very strong anomalous transport and thereby justifying the use of a single-temperature model.

Another interesting dimensionless parameter is the magnetic Reynolds number, the ratio of the resistive diffusion time

TABLE III. Secondary dimensionless parameters for the two stages of pinch implosion.<sup>a</sup>

	$S_1$	$S_2$	$S_3$	$S_4$	$\tau_{rad}/\tau$
1	$8.9 \times 10^{-3}$	$4.3 \times 10^3$	4.65	$1.1 \times 10^{-3}$	81
2	0.18	$1.21 \times 10^5$	692	$5.7 \times 10^{-3}$	134

<sup>a</sup> $S_1$  is the ratio of the drift time to the electron-ion energy equilibration time (Eq. (14));  $S_2$  is the magnetic Reynolds number (Eq. (15));  $S_3$  is the electron magnetization parameter (Eq. (18)); and  $S_4$  is the ratio of the “current” velocity to the ion thermal velocity (Eq. (18)).

over the scale  $a$  ( $a^2/D_M$ , with  $D_M$  being the magnetic diffusion coefficient), to the acoustic time (6). One has:  $D_M = c^2 \nu_{ei}/\omega_{pe}^2$ , where  $\nu_{ei}$  is the electron-ion collision frequency,  $\nu_{ei} = V_{Ti}/\lambda\sqrt{\mu}$ . These relations provide correct dependences of the corresponding quantities on the plasma parameters and are therefore suitable for the scaling studies; the numerical coefficients may differ by a factor of 1.5–2 from the exact values. We denote the magnetic Reynolds number as  $S_2$ . It is

$$a^2/\tau D_M \equiv S_2 = \frac{R_1^2 \beta}{2R_2 \sqrt{\mu}}. \quad (15)$$

The magnetic Reynolds number is very large in all cases (Table III), meaning that magnetic diffusion is insignificant. If convection develops in a high-beta MagLIF plasma, the condition  $S_2 \gg 1$  means that the magnetic field is entrained by the plasma motion and may become tangled.

One can also express in terms of the scaling factors  $R_{1-4}$  the electron magnetization,  $\lambda/\rho_e$ , and the ratio of the relative velocity  $u$  of the electrons and ions (the “current” velocity) to the ion thermal velocity  $v_{Ti}$ . For our scaling purposes, we use the following expressions for  $\rho_e$  and  $u$  (in CGS units):

$$\rho_e = \sqrt{\mu} \rho_i, \quad (16)$$

$$u = (c/4\pi en)|\nabla \times B| = cB/4\pi ena. \quad (17)$$

Using these expressions and Eqs. (2), (3), and (5)–(7), we obtain:

$$\lambda/\rho_e \equiv S_3 = \frac{R_1}{R_2 \sqrt{\pi}}, \quad u/V_{Ti} \equiv S_4 = \frac{2}{\beta R_1}. \quad (18)$$

One sees (Table III) that the electrons are always magnetized,  $S_3 \gg 1$ , and that the current velocity is very small compared to the ion thermal velocity,  $S_4 \ll 1$ , meaning that there are hardly any current-driven micro-instabilities.

To evaluate the role of bremsstrahlung losses, we introduce the cooling time  $\tau_{rad}$  according to definition  $\dot{p}/p = -p/\tau_{rad}$ . A numerical estimate of the thus defined cooling time is<sup>22</sup>

$$\tau_{rad} \text{ (ns)} = \frac{8.9 \times 10^{23} \sqrt{T \text{ (KeV)}}}{n \text{ (cm}^{-3})}. \quad (19)$$

The ratio of this time to the normalization time  $\tau$  (6) can be expressed as a function of the four main scaling parameters and the radius



$$\frac{\tau_{rad}}{\tau} = \frac{1.74 \times 10^5}{R_1} \sqrt{\frac{a}{\beta R_2}}. \quad (20)$$

Note that this ratio depends on  $a$ . Therefore, if we want to have it constant between two systems, we have to make the  $a$  values the same, i.e., the scaled system would become identical to the original one, making useful scaling impossible. This is a general problem of including radiation in hydrodynamic scalings (e.g., Ref. 10). The way around is to assume that radiation is unimportant—as it must be in practical fusion systems, i.e., the ratio (20) must be large. It is indeed large in both regimes 1 and 2, Table III.

One can show that the 2-fluid Braginski equations<sup>21</sup> are invariant with respect to transformations described by Eqs. (8)–(10), provided that the radiative losses are negligible. As an example, we present in Appendix, the proof of scalability for the energy equation. Anomalous transport in high-beta plasma is a three-dimensional phenomenon, which is why it is so hard to simulate it. On the other hand, the scaling approach automatically includes the three-dimensionality of the problem.

#### IV. EXAMPLES OF POSSIBLE SCALED EXPERIMENTS WITH LINEAR PLASMAS

We can now consider a feasibility of scaled experiments that would allow one to address the physics issues of a full-scale experiment but would have some advantages in terms of, say, required energy and/or better diagnostic access. To identify the possible scaled experiments with the same (or close) values of the dimensionless parameters (6), we choose a single dimensional parameter, the plasma radius  $a$ , which we are going to vary, and see how the other dimensional parameters change.

The parameter space corresponding to the pre-heated plasma stage is illustrated by Fig. 1(a). If one holds all the dimensionless parameters constant, a three-fold decrease of the radius (to  $a = 1$  mm) leads to the decrease of the required energy by a factor of 1.7. Other changes include a ten-fold increase of the density,  $\sim$ four-fold increase of the magnetic field, and  $\sim$ four-fold decrease of the time  $\tau$ . These changes would not make the pre-heated plasma much easier.

A more promising path is associated with the fact that the ions during the first stage are un-magnetized,  $R_1 \ll R_2$ . So, some reduction of the parameter  $R_1$  would not have any effect on the plasma confinement and would leave the plasma in the same confinement regime as for the full-scale experiment. As an example, consider the reduction of both  $a$  and  $R_1$  by a factor of 2, leaving all other dimensionless parameters untouched. With that, the plasma energy decreases by a factor of 11 to  $\sim 0.65$  kJ, and the magnetic field decreases by a factor of 1.6 to 0.25 MG. The density remains unchanged, the temperature decreases to  $\sim 200$  eV, and the normalization time decreases to 9 ns. Changes of that scale allow one to perform an experiment on a number of laser and pulsed-power facilities that exist today. Note that, for the plasma parameters of case 1, the change of  $R_1$  does not lead to any significant change of the confinement regime and allows one to address the same physics as that governing the pre-heated plasma formation in a full-scale experiment. The parameter space corresponding to the reduced value of  $R_1$  is shown in Fig. 1(b).

Consider now a possible scaling-down of the experiment on the plasma confinement near the point of the maximum compression. Here, the ions are magnetized,  $R_1 \gg R_2$ . On the other hand, the ratio of the drift frequency for the global mode,  $\omega_D = (\rho_i/a)(V_{Ti}/a)$ , to the ion collision frequency,  $\nu_i = \nu_{Ti}/\lambda$ , is still very small,  $\omega_D/\nu_i = 1/R_1 R_2 \ll 1$ , meaning that we are in the regime of collisional drift instabilities considered in Refs. 15 and 16. This allows us to consider an experiment where the parameter  $R_1$  would be reduced by a factor of 2. The plasma is still strongly magnetized,  $R_1 \gg R_2$ , and at the same time, it remains in the collisional drift-turbulence regime,  $R_1 R_2 \gg 1$ . The ratio  $L/\lambda = R_4 R_2$  is huge,  $\sim 400$ . This allows one to somewhat reduce the parameter  $R_4$ , say, by a modest factor of 2, so that the parallel physics would remain collision-dominated. The parameter domain for the set of parameters in Table II is shown in Fig. 2(a); the parameter domain for the parameters  $R_1$  and  $R_4$  reduced by a factor of 2 is shown in Fig. 2(b).

Even with reduced parameter  $R_4$ , the relative time for the axial redistribution of the plasma,  $L/\tau v_{Ti} = R_4$ , remains greater than one, meaning that the plasma flow through the ends is small. For the radius of  $a = 0.25$  mm, which may provide more space for the plasma diagnostics, the required energy is 11 kJ, the magnetic field is 20 MG, the plasma

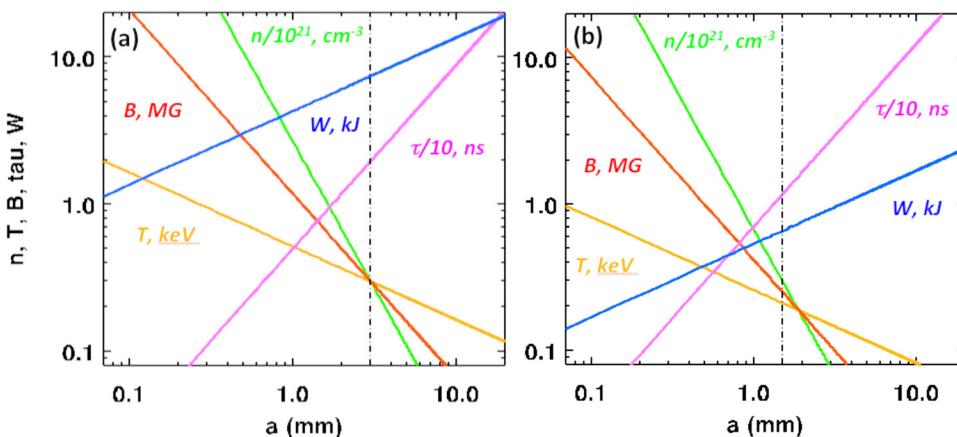


FIG. 1. The parameter domain for the experiments directed towards the study of the early time pre-heated MagLIF plasma (row 1 of Table I): (a) the dimensionless parameters as in row 1 of Table II and (b) the parameter  $R_1$  is half of that of Table II, ( $R_1 = 11.4$ ) with the other parameters held unchanged.

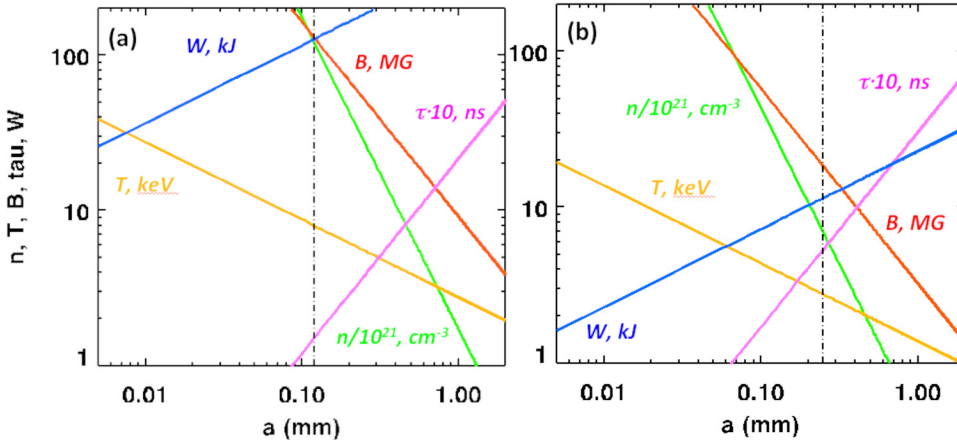


FIG. 2. The parameter domain for the experiments directed towards the study of the MagLIF plasma near stagnation (row 2 of Table I): (a) the dimensionless parameters as in row 2 of Table II and (b) the parameters  $R_1$  and  $R_4$  are reduced by a factor of 2 ( $R_1 = 38.2$  and  $R_4 = 25$ ) with the other parameters held unchanged.

density is  $7.5 \times 10^{21} \text{ cm}^{-3}$ , and the plasma length is 6 mm. These parameters may be attainable using the experiment on the Omega laser facility<sup>23</sup> at the University of Rochester. Peak magnetic fields approaching 40 MG have already been reported by the Omega group.<sup>24</sup> The 40 MG fields were achieved in laser-driven cylindrical implosions with an initial seed magnetic field, although in smaller volumes than we are proposing here.

The plasma parameters in these scaled experiments for the regimes mentioned above are summarized in Table IV. The rows marked as “DT” correspond to an equi-molar DT mixture. The rows marked by “H” correspond to the hydrogen plasma considered in Sec. V.

An approach pursued in our paper could be used as a template for identifying scaled versions of other magnetized target fusion (MTF) systems, in particular, the slow liner implosion on FRC as envisaged in the experiments.<sup>27,28</sup> However, the physics conditions in those experiments are quite different from those of MagLIF. In particular, the plasma beta in these experiments is close to 1. Also, the plasma collisionality expressed in terms of the parameter  $S_l$  is significantly lower (i.e., the parameter  $S_l$  is greater than 1), so that one cannot use the condition  $T_e = T_i$ . The scaling strategy and the set of relevant dimensionless parameters for these systems would be different and would require separate analysis.

Likewise, experiments on laser-driven implosions of the pre-magnetized plasma<sup>25</sup> cannot be described by our approach, as the implosion there occurs at a velocity exceeding the sound speed, and the plasma cannot be considered as simply being in a state of a slowly evolving equilibrium with a slowly moving external confining shell, as is the case for MagLIF and compressed FRCs.

TABLE IV. Parameters of the scaled-down experiments for the two implosion stages.

		$n_e$ $10^{21}$					$T$	$B$	$W$	$\tau$		
$a(\text{mm})$		$R_I$	$R_2$	$R_3$	$R_4$	$\text{cm}^{-3}$	(keV)	(MG)	(kJ)	(ns)	$\tau_{rad}/\tau$	
1	DT	1.5	11.4	333	80.5	2	0.3	0.212	0.252	0.649	11.7	124
	H	1.5	11.4	333	80.5	2	0.12	0.134	0.127	0.164	9.3	325
2	DT	0.24	38.2	7.5	4.57	25	7.5	2.83	19.3	11.5	0.257	351
	H	0.24	38.2	7.5	4.57	25	3	1.79	9.71	2.91	0.204	1150

## V. THE ISOTOPIC EFFECT

Thus far we have been considering the situation where the plasma in the scaled experiment would have the same composition as in a real experiment, where the average atomic mass would be 2.5. The use of tritium in university-scale experiments is not likely, so that a more realistic atomic mass would be 2 (pure deuterium). The difference of the factor of 1.25 does not seem significant for the changes in the plasma confinement regimes and has been ignored in the present analysis. It may, however, be interesting to consider the possibility of switching to a pure hydrogen plasma, where the atomic mass would be 2.5 times less than in a fusion experiment. We, therefore, introduce one more dimensionless parameter into our analysis, the atomic weight  $A = m_i/m_p$ .

Only one of the 4 dimensionless parameters (6),  $R_1$ , is affected by the different atomic mass:  $R_1$  becomes larger for the hydrogen plasma ( $A = 1$ ) by a factor of  $(2.5/A)^{1/2} = (2.5)^{1/2} = 1.58$ . Then, the dependence on the atomic weight propagates through Eqs. (8)–(11). Compared to the initial form, the following factors appear in these equations:  $n \sim (A/2.5)$ ;  $T \sim (A/2.5)^{1/2}$ ;  $B \sim (A/2.5)^{3/4}$ ;  $\tau \sim (A/2.5)^{1/4}$ ; and  $W \sim (A/2.5)^{3/2}$ . Keeping  $R_1$  the same as in the DT experiment and taking  $A = 1$  would, in particular, lead to a reduction of the required energy by a factor of  $(2.5)^{3/2} = 4$ , i.e., to  $\sim 150 \text{ J}$  for the first case and  $\sim 2.9 \text{ kJ}$  for the second case. A summary of these changes is presented in Table IV.

There may also be processes modified by the change of the atomic weight that explicitly depend on the electron mass, like electron parallel thermal conduction and electron magnetization. On the other hand, for the set of parameters considered above both physical processes remain essentially the same: the parallel heat conduction remains negligible, and the electron magnetization remains greater than one.

## VI. DISCUSSION

The scaling analysis presented in this paper demonstrates that the properties of the MagLIF plasmas can be fully imitated in scaled-down experiments. If the four dimensionless parameters defined by Eq. (7) are held approximately the same as in a full-size experiment, one can significantly reduce the required energy and magnetic field and still obtain experimental information pertinent to a full-size experiment.

The absolute values of the plasma parameters and the time scale do change, but the plasma behavior fully replicates the behavior of the initial experiment; such parameters as the confinement time in full-scale experiment can be found by simply changing the time scale according to Eq. (10). Having said that, we have to emphasize that our analysis by itself does not allow one to make *predictions* of the confinement time: it describes, in a rigorous way, a *relation* between the confinement times in two systems, a large one and a much smaller one.

Interestingly, the imploded final stage can be emulated also in an experiment of a much larger scale that would not require multi-megagauss magnetic fields and would not involve any disposable parts. Indeed, if we assume that the plasma radius is 200 times higher than 0.12 mm of Table I, and use hydrogen, we obtain the following set of parameters (Eqs. (8)–(11)):  $n \sim 10^{18} \text{ cm}^{-3}$ ,  $T \sim 0.35 \text{ keV}$ ,  $B \sim 5 \text{ T}$ ,  $W \sim 0.5 \text{ MJ}$ , and  $L \sim 120 \text{ cm}$ . Although the required plasma energy is larger, the characteristic time-scales are much longer, by a factor of  $\sim 10^3$ , according to Eq. (10). In other words, the heating time can be as long as  $1 \mu\text{s}$  ( $1000\tau^*$  of Table I). Such plasmas can, possibly, be created by techniques used in the experiments with the electron-beam heating<sup>26</sup> and field-reversed configuration experiments.<sup>27,28</sup> Referring to experiments,<sup>27,28</sup> we mean that the corresponding pulse-power technology could be used, not that the FRC physics is scalable to the physics of a system with purely axial magnetic field.

It may also be interesting to mention that, if the plasma is heated by a laser or electron beam inside a confining cylinder (a “passive” liner), it may be possible to get some insight into effect of the liner stability on the plasma cooling time in a real system. This could be imitated by machining the inner surface of the liner to create ripples of various amplitudes and wavelengths and studying the effect of these ripples on the plasma lifetime. Such an experiment can provide useful information regarding the effect of the liner waviness on those plasma phenomena whose time-scale is short compared to the growth time of the ripples in a real system.

In summary, we have shown that the scaled-down experiments can correctly reproduce the plasma state at two most critical stages of the whole implosion, the plasma formation early in the pulse, and the stage of a maximum compression. These scaled experiments would require significantly less energy than the full-scale experiment. The goals of such experiment would be to study the process of plasma confinement and to demonstrate fulfillment of the necessary conditions for the success of the whole implosion. Importantly, scaled experiments can be performed with a variety of experimental platforms, not necessarily Z-pinch driven implosions. In particular, a number of issues can be assessed by plasma confined in a stationary cylindrical shell and heated axially by a laser pulse, or heavy-ion-beam, or other technique.

## ACKNOWLEDGMENTS

Work performed for U.S. DoE by LLNL under Contract DE-AC52-07NA27344; Sandia National Laboratories is a multi-program laboratory managed and operated by Sandia

Corporation, a wholly owned subsidiary of Lockheed Martin Corporation, for the U.S. DOE’s NNSA under Contract DE-AC04-94AL85000.

## APPENDIX: SCALABILITY OF TWO-FLUID EQUATIONS

We assume that the initial state of the plasma is known and is characterized by known spatial distributions of density, temperature, and the magnetic field,  $n$ ,  $T$ , and  $\mathbf{B}$ . The initial mass velocities are small, and we neglect them, although at later stage the flows are allowed to develop in the course of the evolution of the plasma state.

We normalize  $n$ ,  $T$ , and  $\mathbf{B}$  to their initial values in the midpoint,  $n_0$ ,  $T_0$ , and  $B_0$ . The spatial coordinates are measured in the units of  $a$ , and the time in the units of  $\tau$  (Eq. (16))

$$\tilde{\mathbf{r}} = \mathbf{r}/a, \quad \tilde{t} = t/\tau. \quad (\text{A1})$$

The parameters  $R_{1-4}$  and  $\tau$  are constructed from  $n_0$ ,  $T_0$ ,  $B_0$ ,  $a$ , and  $L$ .

The normalized equations are formulated in terms of functions  $\tilde{n}(\tilde{\mathbf{r}}, \tilde{t})$ ,  $\tilde{T}(\tilde{\mathbf{r}}, \tilde{t})$ , and  $\tilde{\mathbf{B}}(\tilde{\mathbf{r}}, \tilde{t})$  related to the initial functions by

$$n(\mathbf{r}, t) = n_0 \tilde{n}(\tilde{\mathbf{r}}, \tilde{t}), \quad T(\mathbf{r}, t) = T_0 \tilde{T}(\tilde{\mathbf{r}}, \tilde{t}), \quad \mathbf{B}(\mathbf{r}, t) = B_0 \tilde{\mathbf{B}}(\tilde{\mathbf{r}}, \tilde{t}). \quad (\text{A2})$$

The flow velocity  $\mathbf{v}(\mathbf{r}, t)$  that appears in the course of plasma evolution is normalized as

$$\mathbf{v}(\mathbf{r}, t) = \frac{a}{\tau} \tilde{\mathbf{v}}(\tilde{\mathbf{r}}, \tilde{t}). \quad (\text{A3})$$

For the case of a rapid electron-ion energy exchange, one can sum-up the electron and ion energy Eqs. (2.3e) and (2.3i) of Ref. 21 to obtain

$$3n \left( \frac{\partial T}{\partial t} + \mathbf{v} \cdot \nabla T \right) + 2nT = -\nabla \cdot \mathbf{q} - \pi_{\alpha\beta} \frac{\partial v_\alpha}{\partial x_\beta} + Q_e + Q_i, \quad (\text{A4})$$

where  $\mathbf{q}$  is the heat flux,  $\pi_{\alpha\beta}$  is a viscous stresses tensor, and  $Q$  is the heating power per unit volume, other than viscous heating described by the second term in the right-hand-side. We focus here on the heat flux driven by the temperature gradient; the other terms that we denote by... can be treated identically. The expression for the temperature-driven heat flux is

$$q_\alpha = -\kappa_{\alpha\beta} \frac{\partial T}{\partial x_\beta}. \quad (\text{A5})$$

The general structure of the heat conductivity tensor is:<sup>17</sup>

$$\kappa_{\alpha\beta} = n v_{Ti} \lambda f_{\alpha\beta}(\mu, \rho_i/\lambda), \quad (\text{A6})$$

where  $f_{\alpha\beta}$  are dimensionless functions. [In specific analyses, this expression is used in the form  $\mathbf{q} = -\kappa_{\parallel} \nabla_{\parallel} T - \kappa_{\perp} \nabla_{\perp} T - \kappa_{\wedge} \mathbf{b} \times \nabla T$ .]

By switching to new variables (A2), we have

$$3\tilde{n}\left(\frac{\partial\tilde{T}}{\partial\tilde{t}} + \tilde{\mathbf{v}} \cdot \tilde{\nabla}\tilde{T}\right) + 2\tilde{n}\tilde{T}\tilde{\nabla}\tilde{\mathbf{v}} = -\frac{1}{R_2}\tilde{\nabla} \cdot (g_{\alpha\beta}\tilde{\nabla}\tilde{T}) + \dots, \quad (\text{A7})$$

where

$$g_{\alpha\beta} = \tilde{T}^{5/2} f_{\alpha\beta} \left( \mu, \frac{R_2}{R_1} \frac{\tilde{n}}{\tilde{B}\tilde{T}^{3/2}} \right). \quad (\text{A8})$$

One sees that the two systems, characterized by the same dimensionless scaling parameters, are described by identical equations and are therefore indistinguishable in their behavior, up to the scaling transformations. We have shown this for one of the equations, but one can check that the whole set of Ref. 21 maintains these invariance properties.

<sup>1</sup>S. A. Slutz, M. C. Herrmann, R. A. Vesey, A. B. Sefkow, D. B. Sinars, D. C. Rovang, K. J. Peterson, and M. E. Cuneo, “Pulsed-power-driven cylindrical liner implosions of laser preheated fuel magnetized with an axial field,” *Phys. Plasmas* **17**, 056303 (2010).

<sup>2</sup>M. Shimada, D. J. Campbell, V. Mukhovatov *et al.*, “Progress in the ITER physics basis: Overview and summary,” *Nucl. Fusion* **47**, S1 (2007).

<sup>3</sup>J. D. Lindl “Development of the indirect-drive approach to inertial confinement fusion and the target physics basis for ignition and gain,” *Phys. Plasmas* **2**, 3933 (1995).

<sup>4</sup>M. K. Matzen, B. W. Atherton, M. E. Cuneo *et al.*, “The refurbished Z facility: Capabilities and recent experiments,” *Acta Phys. Pol. A* **115**, 956 (2009).

<sup>5</sup>R. C. Kirkpatrick, I. R. Lindemuth, M. S. Ward, “Magnetized target fusion: An overview,” *Fusion Technol.* **27**, 201 (1995).

<sup>6</sup>R. P. Drake, J. Hammer, C. Hartman *et al.*, “Submegajoule liner implosion of a closed field line configuration,” *Fusion Technol.* **30**, 310 (1996).

<sup>7</sup>R. E. Siemon, I. R. Lindemuth, and K. F. Schoenberg, “Why magnetized target fusion offers a low-cost development path for fusion energy,” *Comments Plasma Phys. Controlled Fusion* **18**, 363 (1999).

<sup>8</sup>G. A. Wurden, T. P. Intrator, P. E. Sieck, “FRCHX magnetized target fusion HEDLP experiments,” *Proc. 2008 Fusion Energy Conference, IAEA, Vienna, 2008*, Paper IC/P4-13 (<http://www-pub.iaea.org/MTCD/Meetings/fec2008pp.asp>).

<sup>9</sup>D. D. Ryutov, R. P. Drake, J. Kane *et al.*, “Similarity criteria for the laboratory simulation of supernova hydrodynamics,” *Astrophys. J.* **518**, 821 (1999).

<sup>10</sup>D. D. Ryutov, B. A. Remington, H. F. Robey, and R. P. Drake, “Magnetohydrodynamic scaling: From astrophysics to the laboratory,” *Phys. Plasmas* **8**, 1804 (2001).

<sup>11</sup>S. A. Slutz, M. R. Douglas, J. S. Lash *et al.*, “Scaling and optimization of the radiation temperature in dynamic hohlraums,” *Phys. Plasmas* **8**, 1673 (2001).

<sup>12</sup>D. B. Sinars, S. A. Slutz, M. C. Herrmann *et al.*, “Measurements of magneto-Rayleigh-Taylor instability growth during the implosion of initially solid Al tubes driven by the 20-MA, 100-ns Z facility,” *Phys. Rev. Lett.* **105**, 185001 (2010).

<sup>13</sup>D. B. Sinars, S. A. Slutz, M. C. Herrmann *et al.*, “Measurements of magneto-Rayleigh-Taylor instability growth during the implosion of initially solid metal liners,” *Phys. Plasmas* **18**, 056301 (2011).

<sup>14</sup>A. ElNadi and M. N. Rosenbluth, “Infinite-beta limit of drift instability,” *Phys. Fluids* **16**, 2036 (1973).

<sup>15</sup>D. D. Ryutov, “On drift instabilities in magnetized target fusion devices,” *Phys. Plasmas* **9**, 4085 (2002).

<sup>16</sup>D. D. Ryutov, D. Barnes, B. Bauer *et al.*, “Particle and heat transport in a dense wall-confined MTF plasma (theory and simulations),” *Nucl. Fusion* **43**, 955 (2003).

<sup>17</sup>N. K. Winsor and D. A. Tidman, “Laser target model,” *Phys. Rev. Lett.* **31**, 1044 (1973).

<sup>18</sup>L. A. Bol’shov, Yu. A. Dreizin, and A. M. Dykhne, “Spontaneous magnetization of electronic thermal conductivity in a laser plasma,” *JETP Lett.* **19**, 168 (1974).

<sup>19</sup>B. D. G. Chandran and S. C. Cowley, “Thermal conduction in a tangled magnetic field,” *Phys. Rev. Lett.* **80**, 3077 (1998).

<sup>20</sup>A. B. Rechester and M. N. Rosenbluth, “Electron heat-transport in a Tokamak with destroyed magnetic surfaces,” *Phys. Rev. Lett.* **40**, 38 (1978).

<sup>21</sup>S. I. Braginski, “Transport processes in a plasma,” in *Reviews of Plasma Physics*, edited by M. A. Leontovich (Consultants Bureau, New York, 1965).

<sup>22</sup>D. L. Book, *NRL Plasma Formulary* (Naval Research Laboratory, 1987).

<sup>23</sup>T. R. Boehly, R. L. McCrory, C. P. Verdon *et al.*, “Inertial confinement fusion experiments with OMEGA-A 30-kJ, 60-beam UV laser,” *Fusion Eng. Des.* **44**, 35 (1999).

<sup>24</sup>J. P. Knauer, O. V. Gotchev, P. Y. Chang *et al.*, “Compressing magnetic fields with high-energy lasers,” *Phys. Plasmas* **17**, 056318 (2010).

<sup>25</sup>P. Y. Chang, G. Fiksel, M. Hohenberger *et al.*, “Fusion yield enhancement in magnetized laser-driven implosions,” *Phys. Rev. Lett.* **107**, 035006 (2011).

<sup>26</sup>A. V. Burdakov, A. V. Arzhannikov, V. T. Astrelin *et al.*, “Concept of fusion reactor based on multiple-mirror trap,” *Fusion Sci. Technol.* **59**, 9 (2011).

<sup>27</sup>T. P. Intrator, G. A. Wurden, W. J. Wagoner *et al.*, “Design and features of the magnetized target fusion experiment,” in *AIP Conference Proceedings of Current Trends in International Fusion Research* (2009), Vol. 1154, p. 65.

<sup>28</sup>R. M. Renneke, T. P. Intrator, S. C. Hsu *et al.*, “Power balance in a high-density field reversed configuration plasma,” *Phys. Plasmas* **15**, 062502 (2008).



Physics of Plasmas is copyrighted by the American Institute of Physics (AIP). Redistribution of journal material is subject to the AIP online journal license and/or AIP copyright. For more information, see <http://ojps.aip.org/pop/popcr.jsp>